# Raman and infrared modes of hydrogenated amorphous carbon nitride

S. E. Rodil, A. C. Ferrari,[a] J. Robertson, and W. I. Milne
*Engineering Department, Cambridge University, Cambridge CB2 1PZ, United Kingdom*

(Received 25 September 2000; accepted for publication 19 February 2001)

Features in the Raman and infrared (IR) spectra of highly $sp^3$ bonded hydrogenated amorphous carbon nitride films are assigned. The Raman spectra show three main features all found in $a$-C itself, the $G$ and $D$ peaks at 1550 and 1350 $cm^{-1}$, respectively, and the $L$ peak near 700 $cm^{-1}$. The intensity ratio of the $D$ and $G$ peaks, $I(D)/I(G)$, is found to scale as $(\text{band gap})^{-2}$, which confirms that nitrogen induces carbon to form $sp^2$ graphitic clusters. The intensity of the $L$ mode is found to scale with the $D$ mode, supporting its identification as an in-plane rotational mode of sixfold rings in graphitic clusters. A small feature at 2200 $cm^{-1}$ due to C≡N modes is seen, but otherwise the Raman spectra resembles that of $a$-C and shows no specific features due to N atoms. The hydrogen content is found to have a strong effect on the IR spectra at 1100–1600 $cm^{-1}$ making this band asymmetric towards the 1600 $cm^{-1}$ region. © *2001 American Institute of Physics.*
[DOI: 10.1063/1.1365076]

## I. INTRODUCTION

Despite numerous efforts, there has been no agreed success in the synthesis of the predicted superhard crystalline phase $C_3N_4$.[1] Nevertheless, there has been considerable effort to make amorphous carbon nitride ($a$-$CN_x$) films.[2] These are wear-resistant films, which are of interest, for example, for coating magnetic hard disks.

$a$-$CN_x$ films can be produced by various deposition methods. The optimization of $a$-$CN_x$ and the related hydrogenated material $a$-$CN_x$:H requires that we can identify the different types of bonding in these films. This is an important task, as N can adopt numerous bonding configurations in carbon nitride with similar stability.[3]

Electron energy loss spectroscopy (EELS) has been an important method to determine the bonding hybridization at the carbon and nitrogen sites, $sp^3$, $sp^2$, or $sp^1$. However, it is a relatively time-consuming technique, and so far it is not able to distinguish between the various nitrogen $sp^2$ configurations.

In $a$-$CN_x$, core level x-ray photoemission spectroscopy is used to probe the configurations of C and N. However, this is partly hindered by the number of configurations and by the small ionicity of the C–N bond, compared to, say, the Si–N bond, so the core level shift due to additional nitrogen is quite small.

Raman and infrared (IR) spectroscopy are widely available, rapid, and nondestructive techniques to probe the bonding. IR absorption arises from vibrational modes with a dipole moment. It is widely used in $a$-C:H to determine the C–H bonding configurations.[4–6] In carbon nitride, IR has identified the N–H stretching modes around 3200 $cm^{-1}$, and this has been used to study the degree of attachment of H to C or N sites.[7] IR has also detected the cyano group C≡N from its mode at 2100 $cm^{-1}$.[8] A very popular idea was that nitrogen introduced into a nonpolar $a$-C network would break the symmetry and give most vibrational modes a significant dipole moment. This would tend to make the IR and Raman spectra similar,[8] as they are in other amorphous covalent solids like $a$-Si.

Raman spectroscopy is now a widely used tool to determine the C–C bonding in all kinds of crystalline and noncrystalline carbons. In most amorphous covalent solids, the Raman spectrum is a weighted version of the vibrational density of states (VDOS) and consists of rather smooth features. The Raman spectra of carbons behave different because Raman scattering from $\pi$ bonding is 50–230 times stronger than from $\sigma$ bonds. In addition, there is a resonant enhancement of two modes, the $G$ and $D$ modes, which causes them to dominate the Raman spectra of disordered carbons, even when the carbons have little graphitic short range order.[9] Amorphous carbon nitride also contains a mixture of $\pi$ and $\sigma$ bonding, so it is expected that $\pi$ bonding will dominate its Raman spectra. This is indeed what occurs.

There are four basic types of carbon nitride films. The first type is $a$-$CN_x$ prepared by reactive sputtering, in which carbon is usually $sp^2$ bonded and nitrogen enhances the carbon $sp^3$ bonding.[10] The second type is $ta$-$CN_x$ prepared by the filtered cathodic vacuum arc (FCVA).[11,12] Here, the carbon is mainly $sp^3$ bonded and the addition of nitrogen causes the carbon to become more $sp^2$ bonded. The third type is $a$-$CN_x$:H prepared by conventional plasma enhanced chemical vapor deposition (PECVD) using source gases such as methane and ammonia or nitrogen.[13] There the carbon atoms have a moderate fraction of $sp^3$ bonds, but the network is not particularly dense or highly connected because of the sizeable fraction of hydrogen. We study the fourth type, $ta$-$CN_x$:H prepared from a high-density plasma source, whose hydrogen content is lower and the $sp^3$ content is higher. We use a source called the electron cyclotron wave resonance source (ECWR),[12] which is a rf powered, inductively coupled PECVD source, operating at low pressure. In this source, the ion current and ion energy are independently controllable.

[a]Electronic mail: acf26@eng.cam.ac.uk

 

The hydrogenated tetrahedral amorphous carbon (*ta*-C:H) films deposited using the ECWR source provides a material with ~30 at. % H and a C-$sp^3$ fraction of 70%.[14,15] It marks a clear difference to previous works where N was incorporated in *a*-C:H films with lower C-$sp^3$ content (~40%).[13,16]

## II. EXPERIMENT

The *ta*-$C_xN_yH_z$ films were deposited onto silicon ⟨100⟩ and Corning glass substrates as a function of the nitrogen to acetylene gas flow ratio ($N_2/C_2H_z$), raising the nitrogen partial pressure up to 85% in the gas phase. The ion energy, on the other hand, was fixed at 80 eV. The elemental composition in the deposited *ta*-$C_xN_yH_z$ films was determined by channeling rutherford backscattering (RBS) and elastic recoil detection analysis (ERDA). The optical gap was derived from transmission and reflection measurements and the conductivity was measured in a coplanar configuration using single gap cells at room temperature and the activation energy was determined by measuring the change in conductivity as a function of the temperature.[17,18]

The bonding was studied by infrared and Raman spectroscopy. The IR spectra were obtained in a vacuum Fourier-transform infrared (FTIR) spectrometer (BOMEM-DA-3) in the 400–4000 $cm^{-1}$ range. A total of 300 scans were used to improve the low signal-to-noise ratio due to the thickness of the films. Unpolarized Raman spectra were recorded in backscattering geometry for 514.5 nm excitation from an Ar ion laser using a Jobin-Yvon T64000 triple grating spectrometer. The resolution was about 3 $cm^{-1}$ and care was taken to avoid sample damage during measurements.

## III. RESULTS

We previously found[17,18] that the nitrogen content in the films increases up to a saturation value of ~30 at. % as the $N_2/C_2H_2$ gas flow ratio increases. The hydrogen content decreases slightly from 30 to 26 at. %. The structural changes caused by nitrogen are seen in the optical, electrical, and IR data. The evolution of the C-$sp^3$ fraction as nitrogen is introduced was obtained using electron energy loss spectroscopy (EELS). Three regions can be distinguished in Fig. 1, where the C-$sp^2$% and optical (Tauc) gap are plotted against the nitrogen content.

(1) Below ~20 at. % N the C-$sp^2$ fraction is constant at 25%–30%, the same as in N-free *ta*-C:H. Nevertheless, the conductivity increases by three orders of magnitude ($5\times10^{-9}$–$4\times10^{-6}$ S $cm^{-1}$), the conductivity activation energy decreases (0.39–0.26 eV), and the optical band gap decreases (1.7–1.4 eV) gradually.

(2) A transition occurs at about 20 at. % N. The C-$sp^2$ fraction increases to about 60% and the optical gap decreases to 1.1 eV.

(3) Higher N contents have no effect on C-$sp^2$ content and gap, but further reduce the conductivity to $10^{-10}$ S $cm^{-1}$. IR shows a preferential bonding of H to N in this region, as olefinic N-containing chains, such as ═N–C, ═N–H, and $RNH_2$ (Fig. 2(a)).

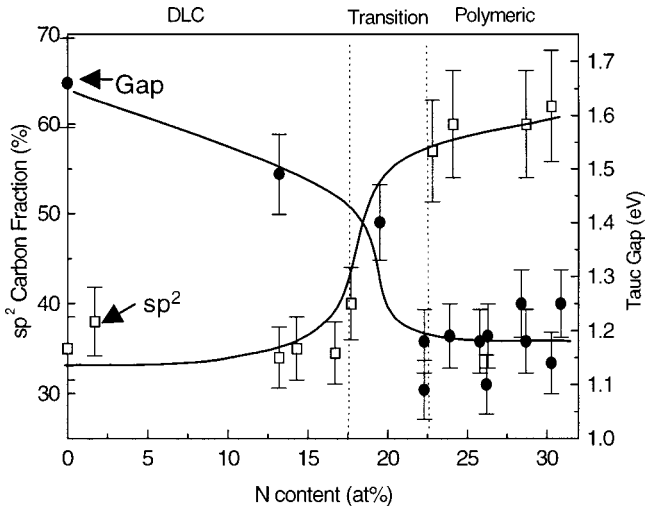


FIG. 1. Variation of the C-$sp^2$% and the optical gap as a function of the N content.

This indicates a transition to more polymeric films. The total H content has not changed much, but the hydrogen has transferred from bonding to C $sp^3$ sites to a preferential bonding in NH groups. This leaves the C in $sp^2$ sites, which leads to the lower optical gap. The mean coordination number of this latter network is much lower, so the films can be scratched and we call them polymeric.

The evolution of the IR spectra can be seen in Fig 2(a). In the N-free *ta*-C:H, the only feature is the C–H stretching band around 2700–3000 $cm^{-1}$. New features emerge when the N content is increased. There are N–H stretching modes around 3300 $cm^{-1}$, a small peak at 2200 $cm^{-1}$ due to the CN $sp^1$ modes, and a broad band around 1000–1600 $cm^{-1}$. The latter becomes asymmetric with a clear peak around 1600 $cm^{-1}$ as the N content increases. Some of the spectra show a sharp peak around 1100 $cm^{-1}$ due to $SiO_2$ present in the silicon wafers before deposition.

Figure 3 shows how the Raman spectra of *ta*-C:N:H films evolve with increasing N content. The spectra are dominated by the *G* and *D* peaks. The *D* and *G* bands are fitted simultaneously by a Breit–Wigner–Fano (BWF) function for the *G* peak and a Lorentzian for the *D* peak. *G* position is given as the maximum of the BWF function rather than its center, to allow comparison with symmetric curve fits.[19]

Three other bands can be observed: (a) a small but well-defined peak (*L*) is seen at ~700 $cm^{-1}$ which increases in intensity as the N content increases; (b) a very broad band near 2000 $cm^{-1}$ at least for the highest N containing samples; and (c) a small sharp C≡N mode at 2200 $cm^{-1}$ is present for most of the N-containing samples.

## IV. INTERPRETATION OF RAMAN FEATURES

In each form of *a*-C, the Raman spectrum is determined by the vibrations of any $sp^2$ sites, because of the resonant enhancement of their scattering. In *a*-C, the *G* peak at 1500–1600 $cm^{-1}$ arises from the bond stretching motion of pairs of $sp^2$ C atoms, in aromatic rings or olefinic chains. The *D*

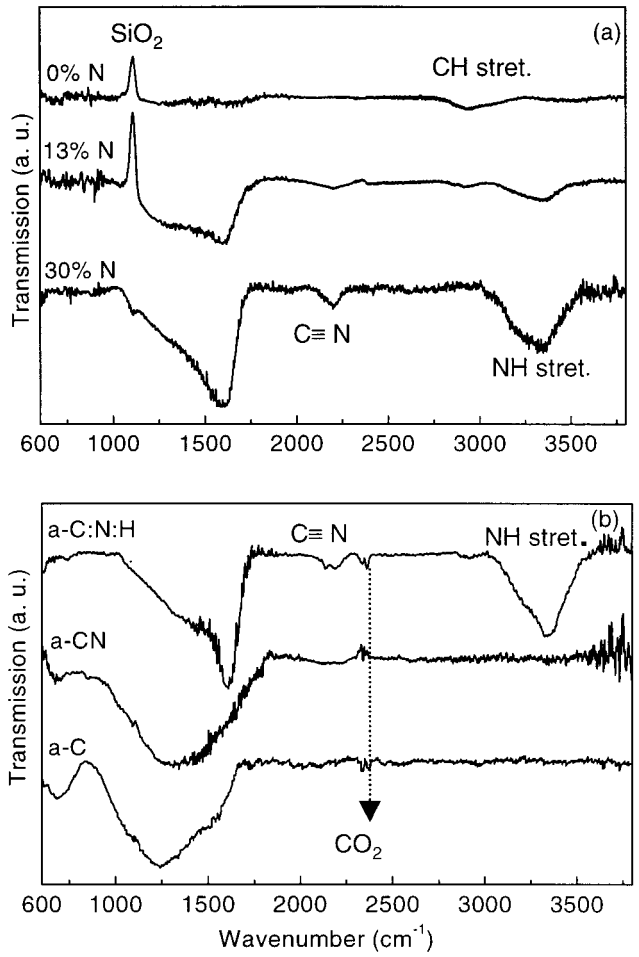


FIG. 2. (a) Infrared spectra of *a*-C:N:H samples with increasing nitrogen content. The spectra have been normalized to the sample thickness. (b) Infrared spectrum of reference samples for comparison. The *a*-C sample was deposited in a magnetron sputtering system, highly $sp^2$ bonded. The *a*-CN sample deposited by the ion assisted FCVA technique has an IR spectrum very similar to the *a*-C sample, even though the nitrogen content is around 30%. Finally, the *a*-C:N:H sample was deposited using the ECWR but using a mixture of $N_2$ and $CH_4$ gases in order to have a higher H content.

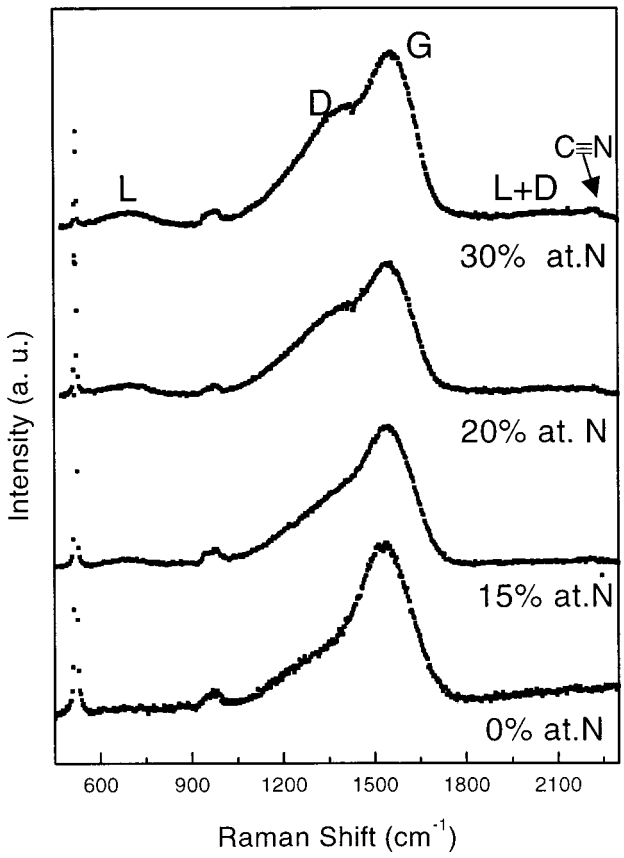


FIG. 3. Raman spectra of *a*-C:N:H samples with different N content. The main features discussed in the article are marked.

band at $\sim$1350 $cm^{-1}$ arises from the breathing modes of $sp^2$ atoms in clusters of six-fold aromatic rings.[19,20]

The position of the *G* mode can vary between 1500 and 1600 $cm^{-1}$. In $sp^2$ bonded *a*-C, the *G* mode is around 1520 $cm^{-1}$, lower than graphite due to bond angle distortions and other disorders which cause a softening of the vibration frequencies. However, the *G* mode moves up with increasing $sp^3$ bonding in *ta*-C ($\sim$1575 $cm^{-1}$) since the remaining $sp^2$ sites change their configuration from rings to short chains and the vibration frequency moves towards the frequency of the C═C dimer embedded in the C–C $sp^3$ matrix. The C═C bond length in the chains is shorter, so the modes lie at higher frequency. In *ta*-C:H, the *G* mode lies around $\sim$1535 $cm^{-1}$, higher than in *a*-C:H of similar gap and $sp^3$ content because some of its $sp^2$ sites are in olefinic $sp^2$ groups rather than in rings.[19]

In microcrystalline graphite, the intensity ratio of the *D* and *G* modes, $I(D)/I(G)$, increases as the grain size decreases.[21] However, for *a*-C the disorder is so great that $I(D)/I(G)$ now decreases with decreasing ''grain'' size.[19] There is no *D* mode if the $sp^2$ sites form only olefinic chains. The presence of the *D* peak in *a*-C indicates that the $sp^2$ sites are forming clusters of fused aromatic rings. The very small *D* peak present in *ta*-C:H film indicates limited clustering of the $sp^2$ sites in rings.

In carbon nitride, as C═C bonds are replaced by C═N bonds, the vibrational frequencies are expected to lie quite close to the mode frequencies in the analogous CN molecule's vibrations (1500–1600 $cm^{-1}$ for chains and 1300–1600 $cm^{-1}$ for rings[22]). The Raman modes are also expected to be quite delocalized over both carbon and nitrogen sites. This means that there is little distinction between modes due to C or N atoms. This explains in general terms why the main features of the Raman spectra resemble those of *a*-C itself.

Now, as the frequency of the skeletal and ring vibrations is relatively constant when comparing benzene with pyridine or pyrrole, it is not easy to assess whether aromatic rings contain nitrogen or not.[23] For rings containing N a contribution between 1400 and 1500 $cm^{-1}$ from N═N vibrations has been suggested,[24] but it seems unphysical at low nitrogen contents. Although the analysis of the Raman spectra of *a*-$CN_x$ could be very difficult, we adopt a simple approach, neglecting, as a first order approximation, the direct contribution of CN vibrations to the spectra. We thus analyze the trends in the *D* and *G* position in the same way as for unnitrogenated samples. If all the trends can be explained in the

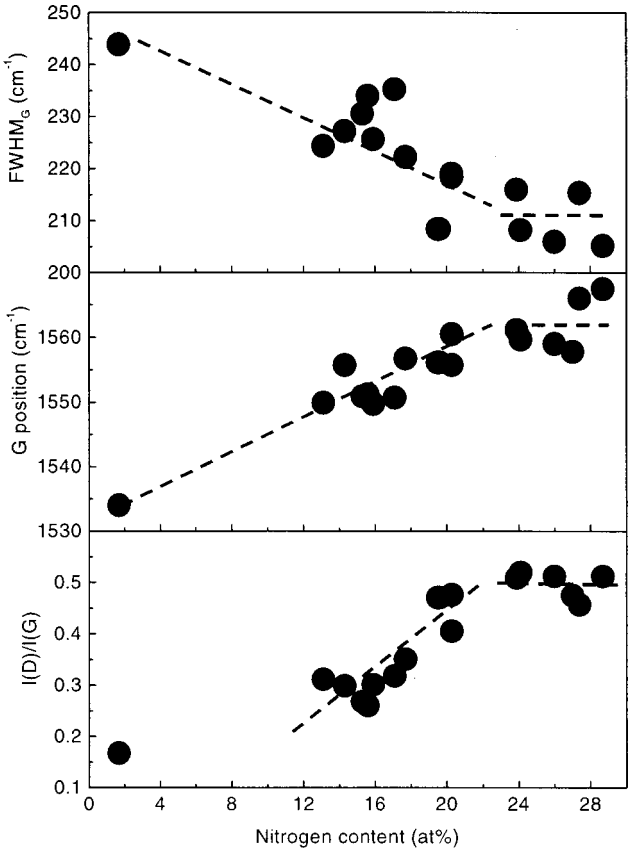


FIG. 4. $G$ width, $G$ position, and $I(D)/I(G)$ ratio vs nitrogen content. The lines are guides to the eye.

same framework of N-free samples, we assume no significant direct contribution of CN or NH vibrations to the Raman spectrum.

Figure 4 shows how $G$ position, $G$ width [full width half maximum (FWHM)], and the $I(D)/I(G)$ ratio change linearly with N content up to N ~20%, being almost independent of N afterwards. A close relationship was found between $I(D)/I(G)$ and the optical gap of $a$-C.[19] Reference 19 proposed that, if the main change in the $sp^2$ phase is due to a clustering of rings, then $I(D)/I(G)$ is proportional to $1/\text{gap}^2$. Figure 5 plots $I(D)/I(G)$ versus $1/E_g^2$. It is seen that a linear relation is followed over the entire range of gaps. This means that with increasing N content the number of aromatic rings per cluster increases. Note also that while the $sp^3$ content has a sharp transition at ~20 at. % N, the Raman parameters change continuously with N content and gap.

A Raman band near 700 cm$^{-1}$ is commonly observed in both $a$-C and $CN_x$ films.[9,25–28] Figure 6(a) shows that the relative intensity of the $L$ band, $I(L)/I(G)$, increases with N content in the same way as the $D$ peak. Note that the $L$ peak was not fitted for the thinner films, as it is not distinguishable from the contribution of the Si combination modes.[29] Figure 6(b) plots the ratio $I(L)/I(G)$ as a function of $I(D)/I(G)$. It shows that there is a linear relation between the intensities of the two bands. This correlation indicates a similar origin of the two modes.

The $L$ band can be associated with a peak in the VDOS of graphite.[20,30] The $L$ mode corresponds to the in-plane rotation of sixfold rings in a graphite layer (Fig. 7).[20] Tamor and Vassel[9] proposed that the $L$ band signifies the absence of hydrogen in $a$-C or $ta$-C films. However, this band is absent in $a$-C:H films of high H content, due to the small $sp^2$ clustering. In contrast, the $L$ band is often observed in N-containing films, even those with 30% H. Indeed the $L$

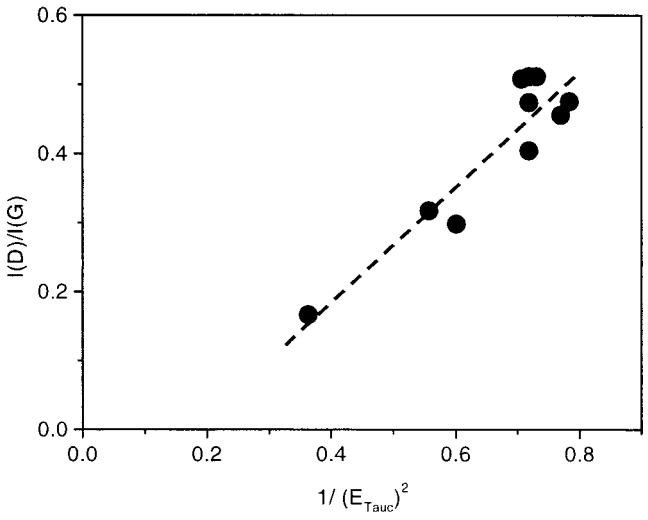


FIG. 5. Linear fit of the $I(D)/I(G)$ ratio vs (optical gap)$^{-2}$ over the entire range of nitrogen contents.

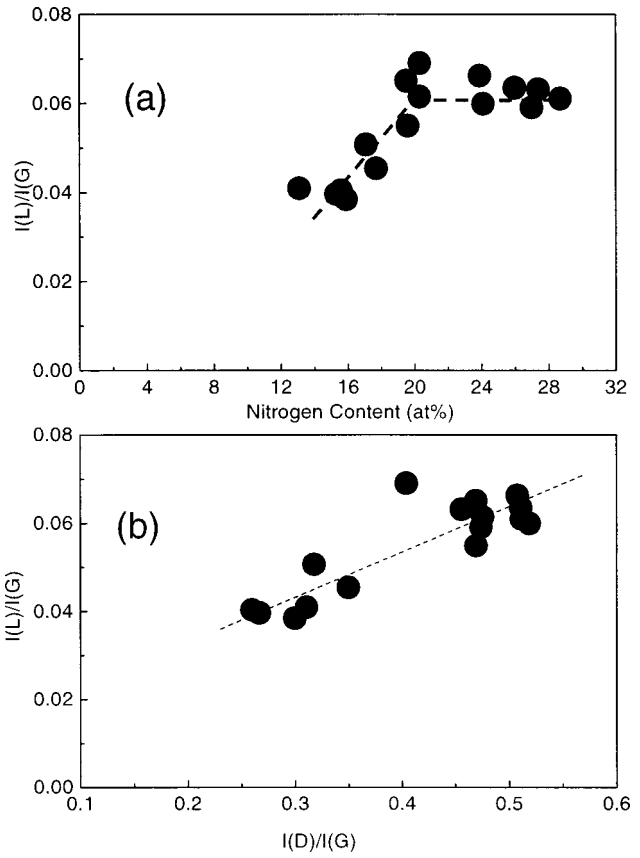


FIG. 6. (a) Variation of the $I(L)/I(G)$ ratio as a function of N content, for samples in which the $L$ peaks could be clearly fitted. (b) Linear correlation between the $I(L)/I(G)$ ratio and the $I(D)/I(G)$ ratio, suggesting a common origin for both peaks.

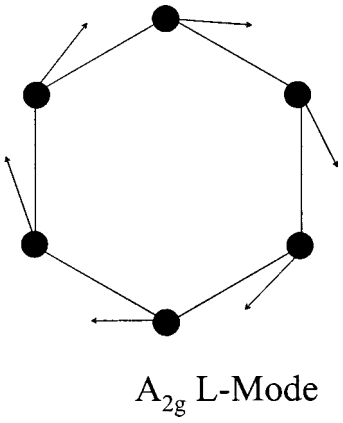


FIG. 7. In-plane rotation mode giving rise to the peak in the phonon density of states of graphite at 700 $cm^{-1}$. Similar modes are found in N-containing rings.

band is observed because N has enhanced the $sp^2$ clustering. This does not mean that it is due to CN related vibrations, even though N-containing rings have strong in-plane bending modes around 700 $cm^{-1}$.[22,23] The other assignment of the *L* modes to pairs of $sp^3$ sites can be ruled out because these would have too small a Raman cross section.[26]

A possible confirmation for the assignment of the 700 $cm^{-1}$ band to $sp^2$ clusters is the broad feature around 2000 $cm^{-1}$, as its intensity follows the same trend as the *D* and *L* bands with the N content. This 2000 $cm^{-1}$ band could be assigned to the combination of 700 and 1300 $cm^{-1}$ vibrations ($L+D$ band), both related with the presence of aromatic rings.

Finally, we assign the peak around 2200 $cm^{-1}$ to C≡N triple bonds.[7,8] This peak is frequently seen in $a$-$CN_x$:H films, but its strength is lower in here. The peak is sometimes masked by the broadband at ~2000 $cm^{-1}$ and so no clear trend with N content could be established. Its intensity is highest at highest N content. However, its relative intensity to the *G* or *D* peaks is very low. This is an important issue because the $sp^1$ concentration is neglected for EELS analysis, based on the low intensity of the CN peak in the IR spectrum.[17,18] Even though we do not have precise figures on the cross section of $sp^1$ vibrations, a very low intensity peak both in FTIR and Raman spectra means that the $sp^1$ contribution is negligible.

It would be desirable to find a Raman feature which could be used to monitor the N content. However, there is so far no one feature that varies in the same systematic way with N in all the carbon nitrides. While various features such as the size of the 2200 $cm^{-1}$ peak or shift of the *G* peak show trends with N content in a particular type of carbon nitride, they show no general trend.

## V. INTERPRETATION OF THE IR SPECTRA

There is no question about the origin of the 3300 and 2200 $cm^{-1}$ bands to N–H stretching modes and C≡N modes, respectively. These assignments have been confirmed by isotopic substitution.[8,31] The interpretation of the broadband at 1100–1600 $cm^{-1}$ relies on the work of Kaufman *et al.*[8] By studying carbon doped samples with different concentrations of $^{14}N$ and $^{15}N$ they conclude that the effect of nitrogen into carbon films is to distort the molecular symmetry of the $sp^2$ rings making the Raman *D* and *G* modes IR active. This conclusion is based on the absence of isotopic shift and the resemblance between the Raman and IR spectra in their samples. However, the similarity between Raman and IR spectra is not generally followed in all types of carbon nitride films.[31,32] Also, a broadband in the 1200–1500 $cm^{-1}$ region is observed in the IR spectra of pure $a$-C (Ref. 33) [Fig. 2(b)], which clearly shows that there are IR-active modes when N is absent.

Here [Fig 2(b)], we note that the strong difference between the IR spectra of H-free $a$-$CN_x$ and $a$-$CN_x$:H is mainly due to the asymmetry of the band towards the 1600 $cm^{-1}$ region in the $a$-$CN_x$:H samples. As a confirmation we deposited $a$-$CN_x$:H samples using $N_2/CH_4$ gas mixtures, in which the H% in the films is higher. We also deposited nonhydrogenated CN samples by ion assisted filtered cathodic arc deposition.[34] A typical IR spectrum of those samples is plotted in Fig. 2(b). This difference between the spectra could be explained by the presence of NH bending modes at 1600 $cm^{-1}$, in agreement with the increment of =N–H and $RNH_2$ modes in $a$-$CN_x$:H samples. However, no significant isotopic shift of this band was observed when substituting H with *D*.[31] Nevertheless, what we want to make clear is that all these arguments put into serious question the assignment of the broadband in the IR spectra to the corresponding 514.5 nm Raman *D* and *G* modes. This is further strengthened by considering that the Raman scattering from carbon films is always a resonant process, with peak positions and intensities changing with the excitation wavelengths.[19] Thus the similarity between the green Raman spectra of certain CNs and their IR spectra has to be considered purely accidental and the Kaufman argument as such can be dismissed. Another approach for the interpretation of the broadband is that it is due to a convolution of C–N and C=N modes and so the increase in the 1600 $cm^{-1}$ peak is related to an increment in the fraction of CN $sp^2$ bonds. However, this does not explain the difference in the spectra of $a$-$CN_x$ and $a$-$CN_x$:H samples and also is not consistent with the lack of isotopic shift by $^{15}N$ substitution.[8,31]

## VI. DISCUSSION

It is important to note that the Raman spectra of $ta$-C films show only a *G* band[19] and $ta$-C:H shows only a very weak *D* peak in addition to the prominent *G* band. The $sp^2$ sites can be induced to form clusters by using higher deposition temperatures[35] or by annealing after deposition.[12,36] The *D* peak will appear even at fixed $sp^3$ content.[36,12,19] The substrate temperature in the present case was always below 50 °C during deposition. Thus the development of the *D* band and the rise in *G* position are due to the N content, suggesting that N induces clustering. Other groups arrived at similar conclusions; the increase in the cluster size was attributed to a decrease in the C–H bonds, as a result of increasing nitrogen, leading to the formation of larger $sp^2$

clusters.[37,38] Alternatively, it has also been proposed that nitrogen acts as a bridge for $sp^2$ domains resulting in an effective enlargement of the cluster size.[39]

Summarizing, we have a series of samples grown at the same ion energy (~80 eV). The N content increases, while the H content is only slightly decreasing. Up to 20% N, the $sp^2$ fraction is roughly constant, but $I(D)/I(G)$ varies as $1/\text{gap}^2$, showing that the $sp^2$ carbon phase is clustering into rings. Infrared spectrum shows an increase of N–H vibrations and a decrease in C–H vibrations, meaning that we have an effective decrease of C–H bonds. The sudden drop in the $sp^3$ fraction at N content over 20% is not paralleled by a sharp change in the Raman parameters and optical band gap, which saturates for N>20%. Thus more N does not increase the $sp^2$ clustering even if there are suddenly more $sp^2$ sites. For these films, the only detectable changes in the vibrational spectra are in the IR spectra, where the broadband around 1500 $cm^{-1}$ becomes asymmetric with a clear peak around 1600 $cm^{-1}$ and the NH stretching band at 3300 $cm^{-1}$ increases, Fig. 2(a).

We can thus think that N is not directly part of the $sp^2$ clusters detected by Raman spectroscopy and that N acts as a bridge between C $sp^2$ and C $sp^3$ sites or that N containing clusters behave similarly to N-free ones. Hydrogen, which usually terminates C $sp^3$ sites in *ta*-C:H, is now preferentially linked to N. At 20% N, the clustering of the C $sp^2$ phase cannot be increased, and the C $sp^3$ formation is no more energetically favorable, due to the chemically induced $sp^2$ hybridization.[34] We end up with C $sp^2$ clusters linked together by CN $sp^2$ structures, with the presence of floppy C≡N and NH bonds.

## VII. CONCLUSIONS

We have found that the trends in Raman spectra of *ta*-$CN_x$:H films can be largely explained in terms of the spectra of N-free *a*-C. The correlation between Raman parameters and N content exists because N induces the clustering of the C-$sp^2$ phase which controls the development of the spectrum. There are specific N related features only at 2200 $cm^{-1}$

The C-$sp^2$ phase orders in rings, and these give rise to the changes in Raman spectra and the optoelectronical properties of carbon nitride films. Therefore the electronic configuration of amorphous carbon nitride samples is similar to that of N-free carbon films, where the $\pi$ bonds (C=C or C=N) control the gap and conductivity.

## ACKNOWLEDGMENTS

This project was funded by the UK Engineering and Physical Science research Council GR/L 16774 I. The authors would like to thank Professor C. E. Bottani of Politecnico di Milano for Raman facilities. S. R. acknowledges financial support from CONACyT and ORS award scheme for a postgraduate scholarship. A. C. F acknowledges funding from a European Union Marie Curie TMR fellowship.

[1] A. M. Liu and M. L. Cohen, Science **24**, 841 (1989); Phys. Rev. B **41**, 10727 (1989).
[2] S. Muhl and J. M. Mendez, Diamond Relat. Mater. **8**, 1809 (1999).
[3] F. Weich, J. Widany, and Th. Frauenheim, Phys. Rev. Lett. **78**, 3326 (1997).
[4] B. Dischler, Europ. Mater. Res. Soc. Symp. Proc. **17**, 189 (1987).
[5] T. Heitz, B. Drévillon, C. Godet, and J. E. Bourée, Phys. Rev. B **58**, 13957 (1998).
[6] J. Ristein, R. T. Stief, L. Ley, and W. Beyer, J. Appl. Phys. **84**, 3836 (1998).
[7] P. Hammer, N. M. Victoria, and F. Alvarez, J. Vac. Sci. Technol. A **16**, 2941 (1998).
[8] J. H. Kaufman, S. Metin, and D. D. Saperstein, Phys. Rev. B **39**, 13053 (1989).
[9] M. A. Tamor and W. C. Vassell, J. Appl. Phys. **76**, 3823 (1994).
[10] N. Hellgren, M. P. Johansson, E. Broitman, L. Hultman, and J. E. Sundgren, Phys. Rev. B **59**, 5162 (1999).
[11] C. A. Davis, D. R. Mackenzie, Y. Yin, E. Kravtchinskaia, G. A. J. Amaratunga, and V. S. Veerasamy, Philos. Mag. B **69**, 1133 (1994).
[12] B. Kleinsorge, A. C. Ferrari, J. Robertson, and W. I. Milne, J. Appl. Phys. **88**, 1149 (2000).
[13] S. R. P. Silva, J. Robertson, G. A. J. Amaratunga, B. Rafferty, L. M. Brown, D. F. Franceschini, and G. Mariotto, J. Appl. Phys. **81**, 2626 (1997).
[14] M. Weiler, K. Lang, E. Li, and J. Robertson, Appl. Phys. Lett. **72**, 1314 (1998).
[15] N. M. Morrison, S. Muhl, S. E. Rodil, A. C. Ferrari, M. Nesladek, W. I. Milne, and J. Robertson, Phys. Status Solidi A **172**, 79 (1999).
[16] J. Schwan, V. Batori, S. Ulrich, H. Ehrhardt, and S. R. P. Silva, J. Appl. Phys. **84**, 2071 (1998).
[17] S. E. Rodil, N. A. Morrison, J. Robertson, and W. I. Milne, Phys. Status Solidi A **174**, 25 (1999).
[18] S. E. Rodil, N. A. Morrison, W. I. Milne, J. Robertson, V. Stolojan, and D. N. Jayawardane, Diamond Relat. Mater. **9**, 524 (2000).
[19] A. C. Ferrari and J. Robertson, Phys. Rev. B **61**, 14095 (2000).
[20] C. Mapelli, C. Castiglioni, G. Zerbi, and K. Mullen, Phys. Rev. B **60**, 12710 (1999).
[21] F. Tunistra and J. L. Koening, J. Chem. Phys. **53**, 1126 (1970).
[22] F. R. Dollish, W. G. Fateley, and F. F. Bentley, *Characteristic Raman Frequencies of Organic Molecules* (Wiley, New York, 1974).
[23] *Physical Methods in Heterocycle Chemistry*, edited by A. R. Katkritzki Academic Press, New York, Vol. II (1963), Vol. IV (1971).
[24] A. K. M. S. Chowdhury, D. C. Cameron, and M. S. J. Hashmi, Thin Solid Films **332**, 62 (1998).
[25] F. Parmigiani, E. Kay, and H. Seki, J. Appl. Phys. **64**, 3031 (1988).
[26] M. Neuhaeuser, H. Hilgers, P. Joeris, R. White, and J. Windeln, Diamond Relat. Mater. **9**, 1500 (2000).
[27] M. Y. Chen, D. Li, X. Lin, V. P. Dravid, Y. Chung, M. Wong, and W. D. Sproul, J. Vac. Sci. Technol. A **11**, 521 (1993).
[28] F. Li and J. S. Lannin, Appl. Phys. Lett. **61**, 2116 (1992).
[29] P. A. Temple and C. E. Hathaway, Phys. Rev. B **7**, 3685 (1973).
[30] R. Al-Jishi and G. Dresselhaus, Phys. Rev. B **26**, 4514 (1982).
[31] N. M. Victoria, P. Hammer, M. C. dos Santos, and F. Alvarez, Phys. Rev. B **61**, 1083 (2000).
[32] J. M. Mendez, A. Gaona-Cuoto, S. Muhl, and S. Jimenez-Sandoval, J. Phys.: Condens. Matter **11**, 5225 (1999).
[33] M. Bonelli, A. P. Fioravanti, A. Miotello, and P. M. Ossi, Europhys. Lett. **50**, 501 (2000).
[34] S. E. Rodil, W. I. Milne, J. Robertson, and L. M. Brown, Appl. Phys. Lett. **77**, 1458 (2000).
[35] M. Chhowalla, A. C. Ferrari, J. Robertson, and G. A. J. Amaratunga, Appl. Phys. Lett. **76**, 1419 (2000).
[36] A. C. Ferrari, B. Kleinsorge, N. A. Morrison, A. Hart, V. Stolojan, and J. Robertson, J. Appl. Phys. **85**, 7191 (1999).
[37] J. Schwan, W. Dworschak, K. Jung, and H. Ehrhardt, Diamond Relat. Mater. **3**, 1034 (1994).
[38] G. Mariotto, F. L. Freire, Jr., and C. A. Achete, Thin Solid Films **241**, 255 (1994).
[39] S. F. Yoon, Rusli, J. Ahn, Q. Zhang, C. Y. Yang, and F. Watt, Thin Solid Films **340**, 62 (1999).